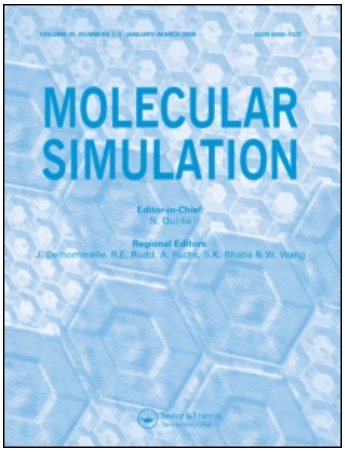

Molecular Simulation
Publication details, including instructions for authors and subscription information:
http://www.informaworld.com/smpp/title~content=t713644482

Structure-based and ligand-based drug design for microsomal prostaglandin E synthase-1 inhibitors

Chia-Ling Li[a]; Tung-Ti Chang[a]; Mao-Feng Sun[b]; Hsin-Yi Chen[c]; Fuu-Jen Tsai[cd]; Mark Fisher[e]; Calvin Yu-Chian Chen[cfg]; Chun-Lin Lee[h]; Wen-Chang Fang[h]; Yung-Hao Wong[e]
[a] Department of Chinese Pediatrics, China Medical University Hospital, Taichung, Taiwan, ROC [b] Department of Acupuncture, China Medical University Hospital, Taichung, Taiwan, ROC [c] Department of Bioinformatics, Asia University, Taichung, Taiwan, ROC [d] Department of Medical Genetics, Pediatrics and Medical Research, China Medical University Hospital and College of Chinese Medicine, China Medical University, Taichung, Taiwan, ROC [e] Harvard-MIT Division of Health Sciences and Technology, Cambridge, MA, USA [f] Laboratory of Computational and Systems Biology, School of Chinese Medicine, China Medical University, Taichung, Taiwan, ROC [g] Computational and Systems Biology, Massachusetts Institute of Technology, Cambridge, MA, USA [h] Department of Business Administration, National Taipei University, Taipei, Taiwan, ROC

Online publication date: 03 March 2011

To cite this Article Li, Chia-Ling , Chang, Tung-Ti , Sun, Mao-Feng , Chen, Hsin-Yi , Tsai, Fuu-Jen , Fisher, Mark , Chen, Calvin Yu-Chian , Lee, Chun-Lin , Fang, Wen-Chang and Wong, Yung-Hao(2011) 'Structure-based and ligand-based drug design for microsomal prostaglandin E synthase-1 inhibitors', Molecular Simulation, 37: 3, 226 — 236
To link to this Article: DOI: 10.1080/08927022.2010.538054
URL: http://dx.doi.org/10.1080/08927022.2010.538054

Molecular Simulation
Vol. 37, No. 3, March 2011, 226–236

Taylor & Francis
Taylor & Francis Group

Structure-based and ligand-based drug design for microsomal prostaglandin E synthase-1 inhibitors

Chia-Ling Li[a†], Tung-Ti Chang[a†], Mao-Feng Sun[b†], Hsin-Yi Chen[c], Fuu-Jen Tsai[cd], Mark Fisher[e], Calvin Yu-Chian Chen[cfg]*, Chun-Lin Lee[h], Wen-Chang Fang[h] and Yung-Hao Wong[f]

[a]*Department of Chinese Pediatrics, China Medical University Hospital, Taichung, Taiwan, ROC;* [b]*Department of Acupuncture, China Medical University Hospital, Taichung, Taiwan, ROC;* [c]*Department of Bioinformatics, Asia University, Taichung 41354, Taiwan, ROC;* [d]*Department of Medical Genetics, Pediatrics and Medical Research, China Medical University Hospital and College of Chinese Medicine, China Medical University, Taichung 40402, Taiwan, ROC;* [e]*Harvard-MIT Division of Health Sciences and Technology, 77 Massachusetts Avenue, Cambridge, MA 02139, USA;* [f]*Laboratory of Computational and Systems Biology, School of Chinese Medicine, China Medical University, Taichung 40402, Taiwan, ROC;* [g]*Computational and Systems Biology, Massachusetts Institute of Technology, Cambridge, MA 02139, USA;* [h]*Department of Business Administration, National Taipei University, Taipei, Taiwan, ROC*

(*Received 31 July 2010; final version received 3 November 2010*)

Microsomal prostaglandin E synthase-1 (mPGES-1) has been regarded as an attractive drug for inflammation-related diseases. In search of new mPGES-1 inhibitors, we performed virtual screening using our traditional Chinese medicine and natural products database (http://tcm.cmu.edu.tw/) and constructed comparative molecular field analysis (CoMFA) and comparative molecular similarity indices analysis (CoMSIA) using a training set of 30 experimentally tested mPGES-1 inhibitors. The CoMFA and CoMSIA models derived were statistically significant with cross-validated coefficient values of 0.808 for CoMFA and 0.829 for CoMSIA and non-cross-validated coefficient values of 0.829 for CoMFA and 0.980 for CoMSIA. Docking and *de novo* evolution design gave three top derivatives, 2-O-caffeoyl tartaric acid-Evo_2, glucogallin-Evo_1 and 3-O-feruloylquinic acid-Evo_7 that have higher binding affinities than the control, glutathione. These three derivatives have interactions with Arg70, Arg73, Arg110, Arg126 and Arg38, which all are mPGES-1 key active site residues. In addition, these derivatives fit well into the CoMFA and CoMSIA models, with hydrophobic, hydrophilic and electropositive substructures mapped onto corresponding contour plots. Hence, we suggest that these three *de novo* compounds could be a starting basis for new mPGES-1 inhibitors.

Keywords: microsomal prostaglandin E synthase-1; QSAR; docking traditional Chinese medicine; database

1. Introduction

In the prostaglandin (PG) biosynthetic pathway, arachidonic acid is converted to PG H2 (PGH2) by cyclooxygenase (COX). PGE2 synthase catalyses the conversion of PGH2 to PG E2 (PGE2), the most abundant PG in the body. PGE2 is an important product of the COX pathway and has been considered as a mediator of inflammation, pain, fever and cancer [1,2]; it is also known to regulate physiological functions in the gastrointestinal tract, in the kidney and in the immune and nervous systems.

Three major isoforms of PGE2 synthases have been identified: cytosolic PG E synthase (cPGES), microsomal PGES 1 (mPGES-1) and mPGES-2 [3,4]. Both cPGES and mPGES-2 are constitutively expressed in various cells and tissues, while mPGES-1 is localised to microsomal compartment of the cell. Recently, mPGES-1 has attracted much attention as a potential drug target for inflammation and pain [5], tumorigenesis, arthritis and atherosclerosis [6], stroke [7,8], cancer [9,10] and tissue repair [11].

Inflammations are related to many diseases, including cancer, arthritis and atherosclerosis. Specifically, mPGES-1 is induced by pro-inflammatory agents and is functionally coupled to COX-2 in various models of inflammation. Previous studies using mPGES-1 knockout mice have shown that mPGES-1 contributes to the inflammatory production of PGE2. Hence, mPGES-1 is a potential drug target for inflammation-related diseases.

Previously, we have investigated mPGES-1 pharmacophore features by Catalyst HypoGen [12], and as a continuation of the project, we applied 3D quantitative structure–activity relationship (3D-QSAR) analysis and molecular docking to search for novel inhibitors for mPGES-1. Both 3D-QSAR and docking techniques are

*Corresponding author. Email: ycc@mail.cmu.edu.tw; ycc929@mit.edu
† All these authors contributed equally to this work.

ISSN 0892-7022 print/ISSN 1029-0435 online

DOI: 10.1080/08927022.2010.538054
http://www.informaworld.com

disciplines of computer-aided drug design (CADD) that have been used in pharmaceutical industry and in our lab for drug development process [13–26].

Aside from employing CADD technologies, we introduced a traditional Chinese medicine (TCM) and natural product database (http://tcm.cmu.edu.tw/) in the virtual screening process. Herbal medicines and natural products have been used in many cultures for hundreds of years, and some have been recently studied to identify the biological activity of the principal components [27–36]. Hence, our goal is to identify natural compounds that possess potential inhibitory activity towards mPGES-1 and that could be further modified for better pharmacological activity.

Table 1. Molecular structure of the training set and the test set

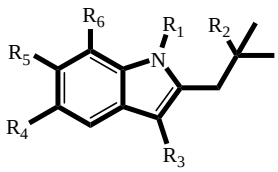

Compound	R1	R2	R3	R4	R5	R6
			Training set			
1	CH2(4-Cl-Ph)	COO–	S-tBu	iPr		H
2	H	COO–	S-tBu	iPr		H
3	Me	COO–	S-tBu	iPr		H
4	CH2(CHdCH2)	COO–	S-tBu	iPr		H
5	(CH2)3Ph	COO–	S-tBu	iPr		H
6	CH2(4-Cl-Ph)	CO2Me	S-tBu	iPr		H
7	CH2(4-Cl-Ph)	CONH2	S-tBu	iPr		H
8	CH2(4-Cl-Ph)	COO–	Ph	iPr		H
9	CH2(4-Cl-Ph)	COO–	OPh	iPr		H
10	CH2(4-Cl-Ph)	COO–	CH2(4-tBu-Ph)	iPr		H
11	CH2(4-Cl-Ph)	COO–	CO(2-Me-Ph)	iPr		H
12	CH2(4-Cl-Ph)	COO–	COCH2S-tBu	iPr		H
13	CH2(4-Cl-Ph)	COO–	COCH2-tBu	iPr		H
14	CH2(4-Cl-Ph)	COO–	Me	iPr		H
15	CH2(4-Cl-Ph)	COO–	Me	H		iPr
16	CH2(4-Cl-Ph)	COO–	Me	H		H
17	CH2(4-Cl-Ph)	COO–	Me	F		H
18	CH2(4-Cl-Ph)	COO–	Me	tBu		H
19	CH2(4-Cl-Ph)	COO–	Me	Ph		H
20	CH2(4-Cl-Ph)	COO–	Me	(3-Ph)-Ph		H
21	CH2(4-Cl-Ph)	COO–	Me	(4-Ph)-Ph		H
22	CH2(4-Cl-Ph)	COO–	Me	(3-Cl,4-Ph)-Ph		H
23	CH2(4-Cl-Ph)	COO–	Me	(3-F,4-Ph)-Ph		H
24	CH2(4-Cl-Ph)	COO–	Me	[3-F,4-(2-MeO–Ph)]-Ph		H
25	CH2(4-Cl-Ph)	COO–	Me	[3-F,4-(2-Cl-Ph)]-Ph		H
26	CH2(4-Cl-Ph)	COO–	Me	[3-F,4-(2-F-Ph)]-Ph		H
27	CH2(4-Cl-Ph)	COO–	Me	[3-F,4-(2-MeCO–Ph)]-Ph		H
28	CH2(4-Cl-Ph)	COO–	Me	[3-F,4-(2-Me-Ph)]-Ph		H
29	CH2(4-Cl-Ph)	COO–	Me	[3-F,4-(3-Me-Ph)]-Ph		H
30	CH2(4-Cl-Ph)	COO–	Me	[3-F,4-(4-Me-Ph)]-Ph		H
			Test set			
31	CH2(4-Cl-Ph)	CO2H	COCH2S-tert-Bu	2-Methyl		H
32	CH2(4-Cl-Ph)	CO2H	COCH2-tert-Bu	2-Methyl		H
33	CH2(4-Cl-Ph)	CO2H	Me	2-Methyl		H
34	CH2(4-Cl-Ph)	CO2H	Me	H		Iso-propyl
35	CH2(4-Cl-Ph)	CO2H	Me	tert-butyl		H
36	CH2(4-Cl-Ph)	CO2H	Me	Ph		H
37	CH2(4-Cl-Ph)	CO2H	Me	Ph		H
38	CH2(4-Cl-Ph)	CO2H	Me	Ph	F	H
39	CH2(4-Cl-Ph)	CO2H	Me	2-MeO–Ph	F	H
40	CH2(4-Cl-Ph)	CO2H	Me	2-Cl-Ph	F	H
41	CH2(4-Cl-Ph)	CO2H	Me	2-MeCO–Ph	F	H
42	CH2(4-Cl-Ph)	CO2H	Me	3-Me-Ph	F	H

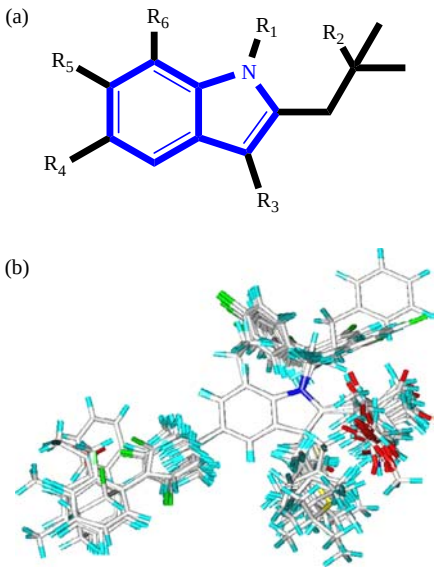

Figure 1. (a) Alignment scaffold for the training set and test set. The core atoms are labelled in bold face blue and (b) the alignment of training set molecules (colour online).

2. Materials and method

2.1 3D quantitative structure–activity relationship

We used SYBYL7.3 (Tripos Inc., St. Louis, MO, USA) to build 3D-QSAR models. Forty-two mPGES-1 inhibitors used in our study were taken from previous literatures [37,38]. The structures of 42 compounds are shown in Table 1. The 2D and 3D structures of these compounds were drawn using ChemBioOffice 2008 (CambridgeSoft Inc., Cambridge, MA, USA) (compound structures shown in Table 1). Structure optimisation was carried out using the MM2 force field. These 42 inhibitors were further divided into the training set and the test set.

The steric and electrostatic energies investigated in comparative molecular field analysis (CoMFA) were calculated by using a carbon probe and a positive charge. Hydrophobic and hydrogen bond donor and acceptor fields were computed in comparative molecular similarity indices analysis (CoMSIA) in addition to steric and electrostatic fields.

2.2 Partial least squares

Partial least squares (PLS) analyses were utilised to analyse the 3D-QSAR models. All CoMFA and CoMSIA fields were regarded as independent variables. By using the leave-one-out method, the value of cross-validation coefficient, q^2, was further employed for non-cross validation to acquire the highest non-cross validation coefficient, r^2, the lowest standard error of estimate, and F-value. The final analysis of the non-cross validation was used to predict the test set activity and to derive the contour maps of CoMFA and CoMSIA.

Table 2. PLS statistics of CoMFA and CoMSIA.

			Cross validation		Non-cross validation		
	CoMFA	CoMSIA	ONC	q^2_{cv}	r^2	SEE	F
ONC	4	A	5	0.052	0.414	1.008	3.391
q^2_{cv}	0.808	E	5	0.466	0.909	0.398	47.715
SEE	0.199	H	6	0.790	0.996	0.088	890.823
r^2	0.976	S	6	0.819	0.976	0.210	154.122
F	255.493	A + D	4	0.077	0.359	1.043	3.493
		A + E	4	0.574	0.900	0.409	56.098
		A + H	5	0.822	0.967	0.241	138.623
		A + S	4	0.818	0.936	0.326	91.982
		E + S	5	0.726	0.969	0.231	151.323
		H + S	6	0.818	0.996	0.082	1028.592
		A + D + E	6	0.475	0.947	0.310	68.447
		A + D + H	6	0.799	0.973	0.219	140.365
		A + D + S	5	0.818	0.938	0.327	73.193
		A + E + S	5	0.743	0.968	0.234	147.395
		A + E + H	6	0.721	0.982	0.181	207.163
		A + H + S	5	0.829	0.980	0.187	232.362
		D + E + S	4	0.668	0.937	0.325	92.306
		E + H + S	4	0.784	0.977	0.196	265.398
		A + D + E + H	5	0.680	0.968	0.234	146.716
		A + D + E + S	5	0.702	0.959	0.267	112.268
		A + D + H + S	4	0.808	0.948	0.293	114.981
		A + E + H + S	6	0.793	0.988	0.145	327.459
		A + D + H + E + S	6	0.761	0.986	0.161	264.192

Notes: ONC, optimal number of component; SEE, standard error of estimate; F, F-test value; PLS, partial least squares; S, steric; E, electrostatic; H, hydrophobic; D, hydrogen bond donor; A, hydrogen bond acceptor

2.3 Docking

Our TCM and natural compound database (http://tcm.cmu.edu.tw/index.php) were used in the docking process. All compounds were drawn using ChemBioOffice 2008 (CambridgeSoft Inc., Cambridge, MA, USA) and energetically minimised in the MM2 forcefield.

All molecular simulations were performed by Discovery Studio 2.5 (Accelrys Inc., San Diego, CA, USA) and CHARMm (Chemistry at Harvard macromolecular mechanics). The protein structure of mPGES-1 was obtained from Protein Data Bank (PDB ID: 3DWW) [39] and employed in the docking study with our laboratory database. The docking procedure first defined the ligand binding site in a receptor before docking ligands into the specified site. LigandFit docking program and scoring functions (DockScore, piecewise linear potential (PLP), potential of mean force (PMF) and LigScore) were used to evaluate the receptor–ligand binding affinity of all compounds and their possible poses. PF-9184 [40], 4-benzo[*b*]thiophen-2-yl-3-bromo-5-hydroxy-5*H*-furan-2-one (BTH) [41] and glutathione were taken as controls for filtering molecules.

2.4 Ligand de novo *evolution*

In *de novo* evolution, derivatives were generated based on existing scaffolds. The Ludi algorithm was used to

Table 3. CoMFA and CoMSIA prediction results of mPGES-1.

	CoMFA			CoMSIA	
Compound	pIC_{50} exp	pIC_{50} pred	Residual	pIC_{50} pred	Residual
1	5.796	5.793	0.003	5.835	-0.039
2	5.000	4.944	0.056	4.781	0.219
3	5.000	4.901	0.099	4.981	0.019
4	5.174	5.146	0.028	5.297	− 0.123
5	5.495	5.688	− 0.193	5.671	− 0.176
6	5.143	5.334	− 0.191	5.068	0.075
7	5.000	5.195	− 0.195	4.897	0.103
8	5.194	5.350	− 0.156	5.397	− 0.203
9	6.187	5.676	0.511	6.156	0.031
10	6.538	6.651	− 0.113	6.561	− 0.023
11	6.046	6.047	− 0.001	6.166	− 0.120
12	6.585	6.554	0.031	6.787	− 0.202
13	6.602	6.620	− 0.018	6.634	− 0.032
14	5.959	6.056	− 0.097	5.957	0.002
15	5.367	5.175	0.192	5.184	0.183
16	5.495	5.577	− 0.082	5.645	− 0.150
17	5.585	5.591	− 0.006	5.601	− 0.016
18	6.481	6.213	0.268	6.109	0.372
19	6.222	6.285	− 0.063	6.302	− 0.080
20	6.796	6.780	0.016	6.796	0.000
21	7.796	8.101	− 0.305	8.009	− 0.213
22	7.658	7.897	− 0.239	7.662	− 0.004
23	8.155	8.183	− 0.028	8.191	− 0.036
24	8.301	8.101	0.201	7.980	0.321
25	8.398	8.125	0.273	8.050	0.348
26	8.097	8.072	0.025	8.093	0.004
27	8.222	8.194	0.028	8.324	− 0.102
28	8.523	8.198	0.325	8.273	0.250
29	7.481	7.654	− 0.173	7.638	− 0.157
30	7.509	7.704	− 0.195	7.760	− 0.251
31	6.585	6.152	0.433	6.655	− 0.070
32	6.602	6.839	− 0.237	6.788	− 0.186
33	5.959	6.600	− 0.641	6.455	− 0.496
34	5.367	5.580	− 0.213	5.286	0.081
35	6.481	6.996	− 0.515	6.899	− 0.418
36	6.222	6.737	− 0.515	6.486	− 0.264
37	6.796	6.938	− 0.142	6.914	− 0.118
38	8.155	8.209	− 0.054	8.254	− 0.099
39	8.301	8.245	0.056	8.250	0.051
40	8.398	8.639	− 0.241	8.411	− 0.013
41	8.222	8.217	0.005	8.174	0.048
42	7.481	6.999	0.482	6.803	0.678

Notes: pIC_{50} exp is experimental pIC_{50}; pIC_{50} pred is predicted pIC_{50}.

evaluate fragments that best complement the receptor. These fragments are fused onto the molecule scaffold, generating a collection of molecules with high Ludi score. Top candidates from previous docking study were taken for *de novo* evolution, and the resultant derivatives were first screened by the Lipinski's rule of five before being docked back to the mPGES-1 active site again for evaluating binding poses and binding affinity.

3. Results and discussion

3.1 3D-QSAR analysis

In this study, we used a training set of 30 compounds to develop our CoMFA and CoMSIA models. All 30 compounds were aligned to core atoms shown in blue in Figure 1(a). The alignment of the training set molecules is shown in Figure 1(b).

PLS analyses of the training set gave a cross-validated coefficient (q^2) value of 0.808, a non-cross-validated coefficient (r^2) of 0.976 and an standard error of estimate (SEE) value of 0.199 for CoMFA (Table 2). As for CoMSIA, the best model (A + H + S) showed a q^2 value of 0.829, an r^2 value of 0.980 and an SEE value of 0.187 (Table 2). The high r^2 and q^2 values and the low SEE value indicate that the 3D-QSAR models are reasonable and should have a good predictive ability.

The predictive ability of the 3D-QSAR models was further verified with an external test set of 12 compounds. The predicted activities of the training and test set molecules were compared with the experimental obser-

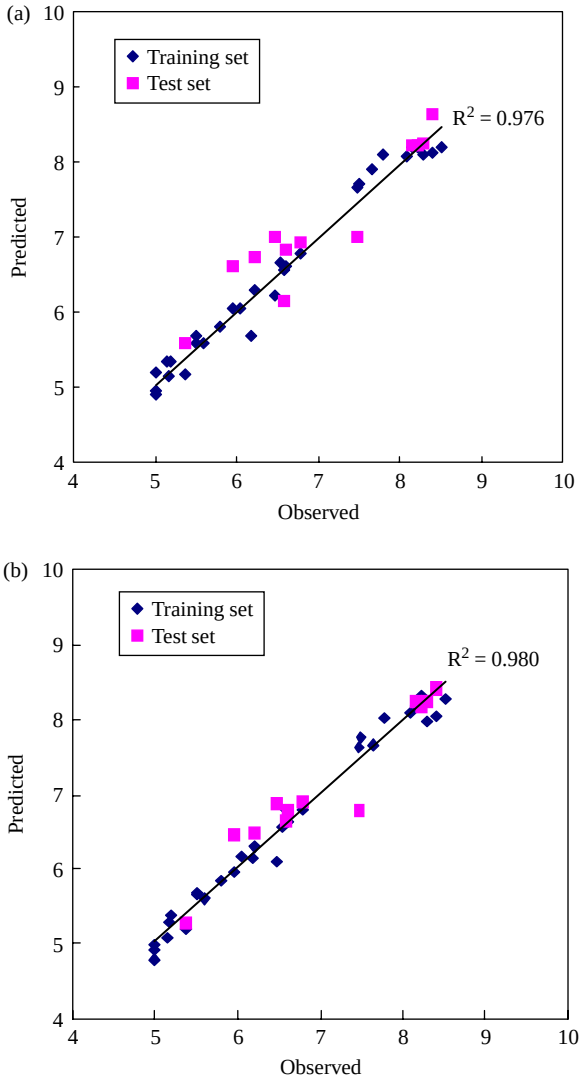

Figure 2. Plot of observed activities versus predicted activities for the training (◆) and test set (■) compounds based on prediction of (a) CoMFA and (b) CoMSIA.

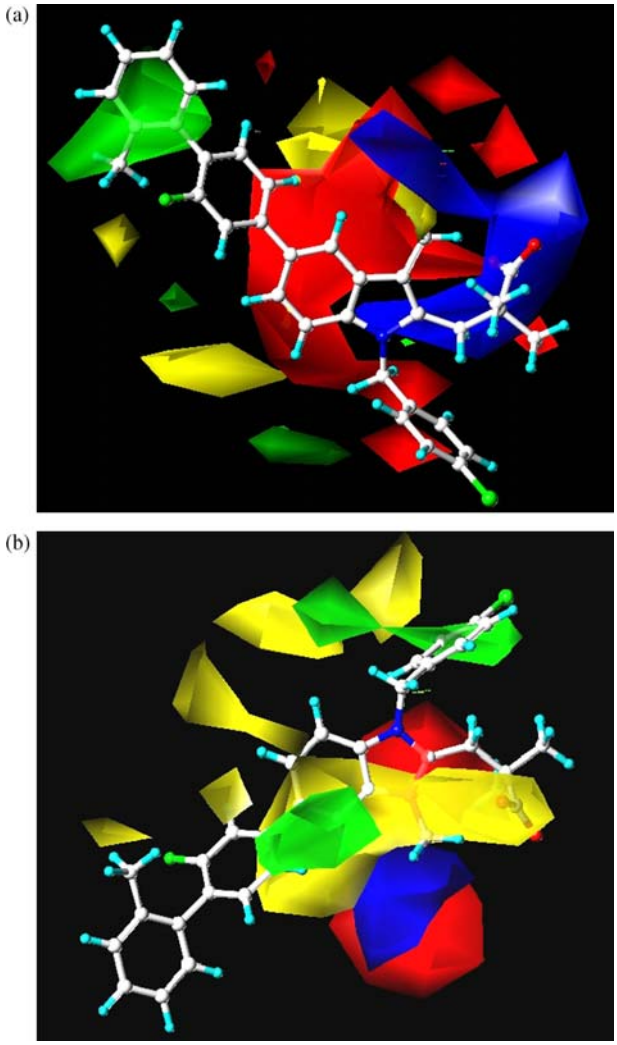

Figure 3. (a) CoMFA contour map. Steric field: favour (green) and disfavour (yellow). Electropositive field: favour (blue) and disfavour (red) and (b) CoMSIA contour map. Hydrophobic field, favour (green) and disfavour (yellow); hydrogen bond acceptor, favour (white) and disfavour (blue); hydrogen bond donor, favour (red) and disfavour (purple) (colour online).

vations (Table 3). As illustrated in Figure 2, the predicted activities for both training and test set compounds showed high correlation with the experimental activities and gave a correlation value (R^2) of 0.976 for CoMFA and 0.980 for CoMSIA. These statistical results suggest that both CoMFA and CoMSIA have good predictions for the training and the test set compounds.

3.2 Contour map analyses of CoMFA

The contour maps of CoMFA and CoMSIA models are shown in Figure 3. The most active training set compound (**28**) is superimposed onto the CoMFA and CoMSIA contours for references. In the CoMFA model (Figure 3(a)), the steric contour maps are represented in green and yellow for favoured and disfavoured contribution, respectively. The large green contour region surrounding the terminal phenyl ring (R4 group) suggests that the steric bulk group could enhance biological activity in this region. This is in good agreement with the experimental results for compounds **19–30**, which all have a terminal phenyl group in this region and all have IC_{50} less than 40 nM. The electrostatic contour maps are shown in red for electronegative contribution and in blue for electropositive contribution. The red contours are found surrounding the terminal phenyl group (R1 group), suggesting that an addition of electronegative substituents could increase biological activity. On the other hand, the blue contours are concentrated near the carboxylate group (R2 group), favouring modification to electropositive group.

3.3 Contour map analyses of CoMSIA

In CoMSIA model, hydrophobic and hydrogen bonding interaction were included in addition to steric and electrostatic field descriptors. In Figure 3(b), the hydrophobic contour maps are shown in green or in yellow for favoured or disfavoured contribution. The hydrogen bond acceptor contour maps are indicated in white for favoured contribution and in blue for the opposite. The contour maps are shown in red or in purple for region favouring or disfavouring hydrogen bond donor. The green contour near the terminal phenyl group (R1 group) indicates that a hydrophobic group in this region is favourable. The yellow contour region near the carboxylate group (R2 group) indicates that a hydrophilic group is favoured. Hence, to enhance the compound activity, we could introduce hydrophobic groups to the terminal phenyl group found at the R1 position and hydrophilic groups to the carboxylate group at the R2 position.

3.4 Docking and de novo *evolution analysis*

In the docking study, the binding affinity between ligands and the receptor was calculated using scoring functions. The DockScores for controls, PF-9184, BTH and glutathione, were 53.466, 54.757 and 66.787, respectively. Preliminary docking experiments resulted in 81 compounds that have DockScores higher than the controls (Table 4; only the top 20 compounds are shown). The top three candidates are 2-O-caffeoyl tartaric acid, chicoric

Table 4. Docking results.

Compound	D.S	PLP1	PLP2	PMF	LigS1	LigS2
2-O-Caffeoyl tartaric acid	215.079	68.06	90.04	224.93	6.64	5.88
Chicoric acid	206.092	117.44	123.46	256.74	7.05	6.05
Mumefural	201.985	72.59	87.65	198.04	6.23	4.96
2-O-Feruloyl tartaric acid	198.739	70.84	83.36	224.55	6.19	5.13
Salvianolic acid B	156.923	110.76	123.01	133.86	7.59	6.83
Rosmarinic acid	148.434	81.92	101.21	223.61	6.79	5.88
Quinic acid	143.961	49.97	60.81	164.90	5.28	4.62
Genipinic acid	142.772	53.24	57.96	195.62	5.65	5.05
Digallic acid	142.547	64.37	81.51	207.53	6.35	5.57
5-O-Feruloylquinic acid	142.462	90.73	101.31	225.85	6.77	5.73
3-O-Feruloylquinic acid	140.488	91.52	106.21	218.68	6.98	5.86
Lithospermic acid	140.305	73.86	111.21	243.55	5.94	3.45
Isochlorogenic acid	140.272	71.80	80.80	228.69	6.45	5.47
Gallic acid	140.219	44.47	53.19	119.23	4.45	4.16
2, 3-Dihydroxycinnamic acid	139.170	42.33	52.25	121.93	4.92	4.29
1-Caffeoylquinic acid	139.057	86.48	92.77	227.00	6.19	5.16
Protocatechuic acid	137.016	38.80	45.62	119.88	4.29	4.18
Shikimic acid	136.811	43.34	50.65	137.44	4.51	4.16
4-O-Caffeoylquinic acid	136.713	81.41	100.12	208.58	6.68	5.50
5-O-Caffeoylshikimic acid	136.493	72.33	89.63	184.15	5.66	4.65
PF-9184	53.466	93.82	100.17	175.53	5.27	6.21
BTH	54.757	61.90	59.57	103.39	4.39	4.76
Glutathione	66.787	102.17	98.17	193.40	7.02	6.28

Notes: D.S, Dock score; LigS1, LigScore1; LigS2, LigScore2; only the top 20 candidates and controls are shown.

Table 5. Docking results for *de novo* products.

Compound	D.S	PLP1	PLP2	PMF	LigS1	LigS2
2-O-Caffeoyl tartaric acid-Evo_2	222.198	87.60	98.80	196.39	6.24	5.43
Glucogallin-Evo_1	169.762	86.96	107.38	243.42	7.03	6.14
3-O-Feruloylquinic acid-Evo_7	167.056	95.10	111.99	234.69	7.13	6.09
1-Caffeoylquinic acid-Evo_3	165.916	94.30	101.14	240.61	6.62	5.12
3-O-Feruloylquinic acid-Evo_5	159.929	96.61	116.46	250.69	7.27	5.99
Capillartemisin B-Evo_4	152.081	90.53	101.68	216.51	6.28	4.17
Capillartemisin B-Evo_1	151.803	94.49	106.10	222.5	6.30	4.02
Capillartemisin B-Evo_6	150.856	84.49	95.74	213.4	6.25	4.14
Gentisic acid-Evo_1	146.487	57.94	60.68	151.53	4.90	4.83
3-O-Feruloylquinic acid-Evo_2	145.552	87.65	97.85	248.49	6.17	5.08
O-Coumaric acid-Evo_2	145.117	63.83	71.65	155.32	5.64	4.98
Capillartemisin B-Evo_5	144.76	87.00	94.31	203.15	5.46	3.84
Capillartemisin B-Evo_2	144.719	87.51	96.51	200.48	5.49	3.83
O-Coumaric acid-Evo_1	144.069	64.43	73.19	148.43	5.64	5.04
Picrocrocinic acid-Evo_1	141.492	93.51	110.13	242.07	6.18	3.96
3-O-Feruloylquinic acid-Evo_3	141.444	86.44	99.14	237.14	7.15	5.86
O-Coumaric acid-Evo_5	141.085	58.98	65.56	142.49	5.46	4.76
Caffeic acid-Evo_1	140.641	37.91	52.82	133.02	4.88	4.63
3,5-Dihydroxycinnamic acid-Evo_1	139.832	37.91	52.82	131.04	4.88	4.63
Ferulic acid-Evo_5	139.070	56.55	67.36	151.75	5.91	5.16

Note: The top 20 candidates are shown here.

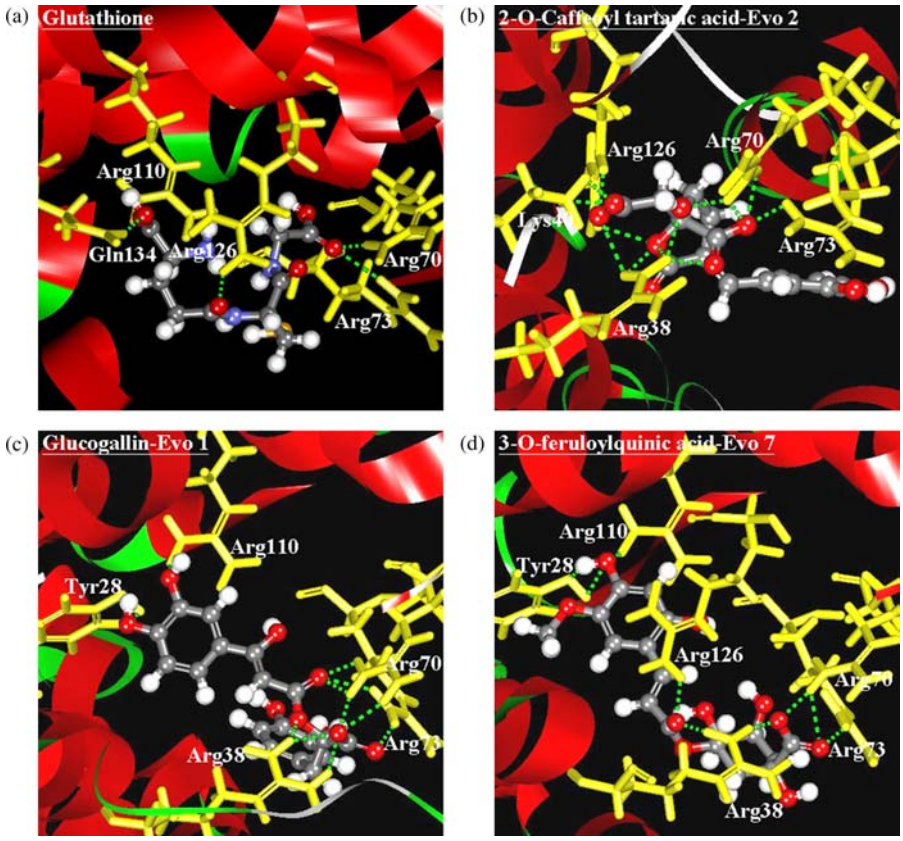

Figure 4. Binding conformation of (a) Glutathione, (b) 2-O-Caffeoyl tartaric acid-Evo_2, (c) Glucogallin-Evo_1 and (d) 3-O-Feruloylquinic acid-Evo_7 at the mPGES-1 binding site.

Table 6. Number of hydrogen bonds formed between ligands and mPGES-1 active site residues.

Compound	Arg70	Arg73	Arg110	Arg126	Gln134	Tyr28	Arg38	Lys42
Glutathione	1	1	1	1	1	–	–	–
2-O-Caffeoyl tartaric acid-Evo_2	3	1	–	3	–	–	5	2
Glucogallin-Evo_1	4	2	1	–	–	2	3	–
3-O-Feruloylquinic acid-Evo_7	2	1	1	1	–	2	2	–

acid and mumefural, and their DockScores are 215.079, 206.092 and 201.985, respectively.

A total of 408 derivatives were generated based on the top compounds obtained from the previous docking step. Only 50 derivatives that passed Lipinski's rule of five were docked back to the mPGES-1 binding site. The top 20 *de novo* compounds, ranked in order of their DockScores, are shown in Table 5. The top three *de novo* compounds are 2-O-caffeoyl tartaric acid-Evo_2, glucogallin-Evo_1 and 3-O-feruloylquinic acid-Evo_7, and their DockScores are 222.198, 169.762 and 167.056, respectively.

The binding conformation of glutathione (control) and the top three derivatives are illustrated in Figure 4, which shows ligands forming hydrogen bond interactions with residues Arg70, Arg73, Arg110, Arg126 and Arg38. All these residues have been identified as key active site residues in previously published studies [42–45]. A summary of the number of hydrogen bonds formed between the ligands and mPGES-1 residues is shown in Table 6. All the top three derivatives have greater number of hydrogen bonds than the control, thus providing a possible explanation for their elevated DockScores.

3.5 CoMFA and CoMSIA mapping

The top three derivatives mapped onto the CoMFA and CoMSIA models are shown in Figures 5 and 6. The common features of the three derivatives are shown in Figure 7, with red circles indicating characteristics noticed from CoMFA and blue circles for features obtained from CoMSIA. Red circle 1 indicates the site having electropositive features, and red circle 2 indicates the region favouring steric bulk group. Blue circle 1 indicates the region having hydrophobic features, and blue circle 2 represents the site favouring hydrophilic features. As shown in the docking results, all substructures circled by blue circle 2 could form strong hydrogen bonding interactions with the receptor. Therefore, the presence of hydrophilic groups could be a big influence for mPGES-1 inhibitor activity. In addition, the hydrophobic substructure of these three derivatives (circled by blue circle 1) could form hydrophobic interactions with other surrounding residues which further strengthen binding interactions. Based on these findings, these functional groups are suggested to be key factors in designing mPGES-1 inhibitors.

4. Conclusions

Several novel anti-cancer or anti-inflammatory compounds were investigated from TCM [46–48]. So, we introduced a TCM database (http://tcm.cmu.edu.tw/) into our research. Derivative, 2-O-Caffeoyl tartaric acid-Evo_2, has the highest DockScore of the 50 *de novo*

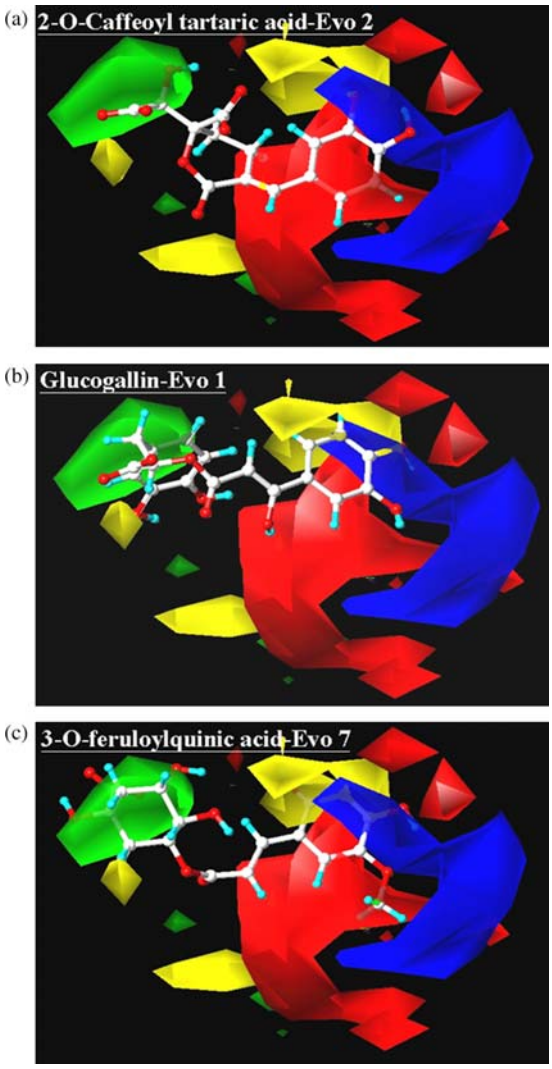

Figure 5. Mapping of *de novo* compounds to CoMFA model. The selected compounds are (a) 2-O-Caffeoyl tartaric acid-Evo_2, (b) Glucogallin-Evo_1 and (c) 3-O-Feruloylquinic acid-Evo_7. Steric field, favour (green) and disfavour (yellow); electropositive field, favour (blue) and disfavour (red) (colour online).

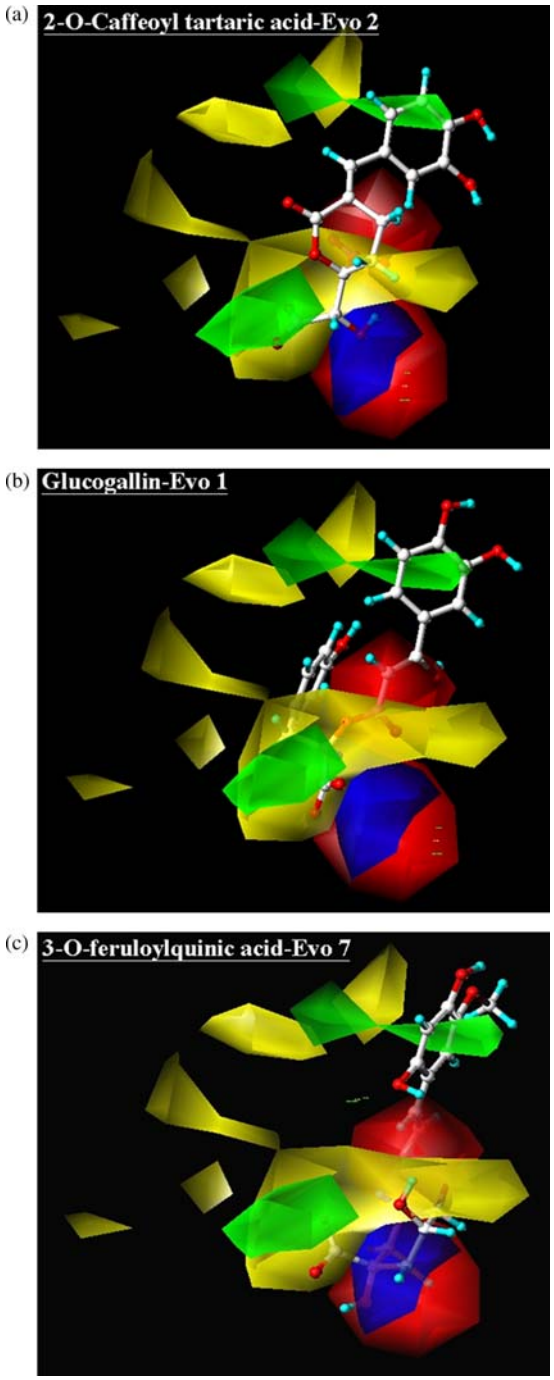

Figure 6. Mapping of *de novo* compounds to CoMSIA model. The selected compounds are (a) 2-O-Caffeoyl tartaric acid-Evo_2, (b) Glucogallin-Evo_1 and (c) 3-O-Feruloylquinic acid-Evo_7. Hydrophobic field, favour (green) and disfavour (yellow); hydrogen bond acceptor, favour (white) and disfavour (blue); hydrogen bond donor, favour (red) and disfavour (purple) (colour online).

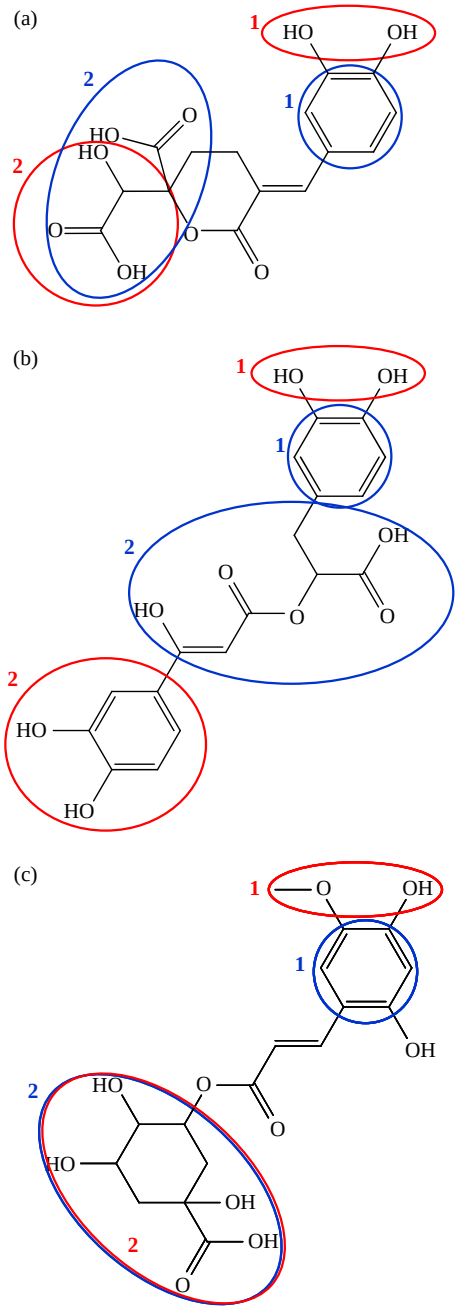

Figure 7. Common features observed among the top derivatives: (a) 2-O-Caffeoyl tartaric acid-Evo_2, (b) Glucogallin-Evo_1 and (c) 3-O-Feruloylquinic acid-Evo_7. Red circle 1 indicates electropositive characteristics; red circle 2 indicates steric favour region. Blue circle 1 indicates hydrophobic features; blue circle 2 indicates hydrophilic features. The red circles are features observed from CoMFA ligand mapping, while the blue circles are obtained from CoMSIA ligand mapping (colour online).

products, and its original compound (2-O-Caffeoyl tartaric acid) also ranks first in the preliminary docking. The top three derivatives, 2-O-caffeoyl tartaric acid-Evo_2, glucogallin-Evo_1 and 3-O-feruloylquinic acid-Evo_7, interact with five key mPGES-1 residues, Arg70, Arg73, Arg110, Arg126 and Arg38, respectively. These derivatives mapped well onto the CoMFA and CoMSIA models, and four common chemical features could be observed

from these three derivatives. Overall, we hope that the above findings will provide a constructive idea for designing mPGES-1 inhibitors.

Acknowledgements

The research was supported by grants from the National Science Council of Taiwan (NSC 99-2221-E-039-013-), China Medical University (CMU98-TCM, CMU99-S-02) and Asia University (CMU98-ASIA-09). This study was also supported in part by Taiwan Department of Health Clinical Trial and Research Center of Excellence (DOH99-TD-B-111-004) and Taiwan Department of Health Cancer Research Center of Excellence (DOH99-TD-C-111-005). We are grateful to the National Center of High-performance Computing for computer time and facilities.

References

[1] J.I. Kim, V. Lakshmikanthan, N. Frilot, and Y. Daaka, *Prostaglandin E2 promotes lung cancer cell migration via EP4-betaArrestin1-c-Src signalsome*, Mol. Cancer Res. 8 (2010), pp. 569–577.

[2] N. Li, M.A. Rivera-Bermudez, M. Zhang, J. Tejada, S.S. Glasson, L.A. Collins-Racie, E.R. Lavallie, Y. Wang, K.C. Chang, S. Nagpal, E.A. Morris, C.R. Flannery, and Z. Yang, *LXR modulation blocks prostaglandin E2 production and matrix degradation in cartilage and alleviates pain in a rat osteoarthritis model*, Proc. Natl. Acad. Sci. USA 107 (2010), pp. 3734–3739.

[3] S. Hara, D. Kamei, Y. Sasaki, A. Tanemoto, Y. Nakatani, and M. Murakami, *Prostaglandin E synthases: Understanding their pathophysiological roles through mouse genetic models*, Biochimie 92 (2010), pp. 651–659.

[4] S. Mattila, H. Tuominen, J. Koivukangas, and F. Stenback, *The terminal prostaglandin synthases mPGES-1, mPGES-2, and cPGES are all overexpressed in human gliomas*, Neuropathology 29 (2009), pp. 156–165.

[5] M. Dallaporta, E. Pecchi, S. Thirion, A. Jean, and J.D. Troadec, *Toward the management of inflammation: Recent developments of mPGES-1 inhibitors*, Recent Pat. CNS Drug Discov. 5 (2010), pp. 70–80.

[6] M. Wang, W.L. Song, Y. Cheng, and G.A. Fitzgerald, *Microsomal prostaglandin E synthase-1 inhibition in cardiovascular inflammatory disease*, J. Intern. Med. 263 (2008), pp. 500–505.

[7] Y. Ikeda-Matsuo, A. Ota, T. Fukada, S. Uematsu, S. Akira, and Y. Sasaki, *Microsomal prostaglandin E synthase-1 is a critical factor of stroke-reperfusion injury*, Proc. Natl. Acad. Sci. USA 103 (2006), pp. 11790–11795.

[8] Y. Ikeda-Matsuo, Y. Hirayama, A. Ota, S. Uematsu, S. Akira, and Y. Sasaki, *Microsomal prostaglandin E synthase-1 and cyclooxygenase-2 are both required for ischaemic excitotoxicity*, Br. J. Pharmacol. 159 (2010), pp. 1174–1186.

[9] H. Hanaka, S.C. Pawelzik, J.I. Johnsen, M. Rakonjac, K. Terawaki, A. Rasmuson, B. Sveinbjornsson, M.C. Schumacher, M. Hamberg, B. Samuelsson, P.J. Jakobsson, P. Kogner, and O. Radmark, *Microsomal prostaglandin E synthase 1 determines tumor growth* in vivo *of prostate and lung cancer cells*, Proc. Natl. Acad. Sci. USA 106 (2009), pp. 18757–18762.

[10] D. Kamei, M. Murakami, Y. Sasaki, Y. Nakatani, M. Majima, Y. Ishikawa, T. Ishii, S. Uematsu, S. Akira, S. Hara, and I. Kudo, *Microsomal prostaglandin E synthase-1 in both cancer cells and hosts contributes to tumour growth, invasion and metastasis*, Biochem. J. 425 (2009), pp. 361–371.

[11] K. Gudis, A. Tatsuguchi, K. Wada, S. Futagami, K. Nagata, T. Hiratsuka, Y. Shinji, K. Miyake, T. Tsukui, Y. Fukuda, and C. Sakamoto, *Microsomal prostaglandin E synthase (mPGES)-1, mPGES-2 and cytosolic PGES expression in human gastritis and gastric ulcer tissue*, Lab. Invest. 85 (2005), pp. 225–236.

[12] C.Y.C. Chen, *Pharmacoinformatics approach for mPGES-1 in anti-inflammation by 3D-QSAR pharmacophore mapping*, J. Taiwan Inst. Chem. Eng. 40 (2009), pp. 155–161.

[13] Y.C. Chen and K.T. Chen, *Novel selective inhibitors of hydroxyxanthone derivatives for human cyclooxygenase-2*, Acta Pharmacol. Sin. 28 (2007), pp. 2027–2032.

[14] C.Y.C. Chen, *Discovery of novel inhibitors for c-Met by virtual screening and pharmacophore analysis*, J. Chin. Inst. Chem. Eng. 39 (2008), pp. 617–624.

[15] C.Y.C. Chen, *A novel perspective on designing the inhibitor of HER2 receptor*, J. Chin. Inst. Chem. Eng. 39 (2008), pp. 291–299.

[16] C.Y.C. Chen, *Insights into the suanzaoren mechanism – From constructing the 3D structure of GABA-A receptor to its binding interaction analysis*, J. Chin. Inst. Chem. Eng. 39 (2008), pp. 663–671.

[17] C.Y.C. Chen, *Chemoinformatics and pharmacoinformatics approach for exploring the GABA-A agonist from Chinese herb suanzaoren*, J. Taiwan Inst. Chem. Eng. 40 (2009), pp. 36–47.

[18] Y.C. Chen, *The molecular dynamic simulation of zolpidem interaction with gamma aminobutyric acid type A receptor*, J. Chin. Chem. Soc. 54 (2007), pp. 653–658.

[19] C.Y. Chen, Y.H. Chang, D.T. Bau, H.J. Huang, F.J. Tsai, and C.H. Tsai, *Ligand-based dual target drug design for H1N1: Swine flu – A preliminary first study*, J. Biomol. Struct. Dyn. 27 (2009), pp. 171–178.

[20] C.Y.C. Chen, De novo *design of novel selective COX-2 inhibitors: From virtual screening to pharmacophore analysis*, J. Taiwan Inst. Chem. Eng. 40 (2009), pp. 55–69.

[21] C.Y.C. Chen, G.W. Chen, and W.Y.C. Chen, *Molecular simulation of HER2/neu degradation by inhibiting HSP90*, J. Chin. Chem. Soc. 55 (2008), pp. 297–302.

[22] C.Y. Chen, Y.H. Chang, D.T. Bau, H.J. Huang, F.J. Tsai, C.H. Tsai, and C.Y.C. Chen, *Discovery of potent inhibitors for phosphodiesterase 5 by virtual screening and pharmacophore analysis*, Acta Pharmacol. Sin. 30 (2009), pp. 1186–1194.

[23] C.Y.C. Chen, *Weighted equation and rules – A novel concept for evaluating protein–ligand interaction*, J. Biomol. Struct. Dyn. 27 (2009), pp. 271–282.

[24] C.Y.C. Chen, *Computational screening and design of traditional Chinese medicine (TCM) to block phosphodiesterase-5*, J. Mol. Graph. Model. 28 (2009), pp. 261–269.

[25] C.Y.C. Chen, *Insights into designing the dual-targeted HER2/HSP90 inhibitors*, J. Mol. Graph. Model. 29 (2010), pp. 21–31.

[26] C.Y.C. Chen, *Bioinformatics, chemoinformatics, and pharmainformatics analysis of HER2/HSP90 dual-targeted inhibitors*, J. Taiwan Inst. Chem. Eng. 41 (2010), pp. 143–149.

[27] C.D. Yoo, S.C. Kim, and S.H. Lee, *Molecular dynamics simulation study of probe diffusion in liquid n-alkanes*, Mol. Simul. 35 (2009), pp. 241–247.

[28] D.X. Li, G.L. Chen, B.L. Liu, and Y.S. Liu, *Molecular simulation of -cyclodextrin inclusion complex with 2-phenylethyl alcohol*, Mol. Simul. 35 (2009), pp. 199–204.

[29] F. Luan, H.T. Liu, Y. Gao, and X.Y. Zhang, *QSPR model to predict the thermal stabilities of second-order nonlinear optical (NLO) chromophore molecules*, Mol. Simul. 35 (2009), pp. 248–257.

[30] J.H. Jing, G.Z. Liang, H. Mei, S.Y. Xiao, Z.N. Xia, and Z.L. Li, *Quantitative structure–mobility relationship studies of dipeptides in capillary zone electrophoresis using three dimensional holographic vector of atomic interaction field*, Mol. Simul. 35 (2009), pp. 263–269.

[31] A.M. Al-Mekhnaqi, M.S. Mayeed, and G.M. Newaz, *Prediction of protein conformation in water and on surfaces by Monte Carlo simulations using united-atom method*, Mol. Simul. 35 (2009), pp. 292–300.

[32] M.L. Mihajlovic and P.M. Mitrasinovic, *Applications of the ArgusLab4/AScore protocol in the structure-based binding affinity prediction of various inhibitors of group-1 and group-2 influenza virus neuraminidases (NAs)*, Mol. Simul. 35 (2009), pp. 311–324.

[33] K. Roy and G. Ghosh, *QSTR with extended topochemical atom (ETA) indices. 11. Comparative QSAR of acute NSAID cytotoxicity in rat hepatocytes using chemometric tools*, Mol. Simul. 35 (2009), pp. 648–659.

[34] P. Nimmanpipug, V.S. Lee, P. Wolschann, and S. Hannongbua, *Litchi chinensis-derived terpenoid as anti-HIV-1 protease agent: Structural design from molecular dynamics simulations*, Mol. Simul. 35 (2009), pp. 673–680.

[35] P. Ghosh and M.C. Bagchi, *Comparative QSAR studies of nitrofuranyl amide derivatives using theoretical structural properties*, Mol. Simul. 35 (2009), pp. 1185–1200.
[36] Y.S. Zhao, Q.C. Zheng, H.X. Zhang, H.Y. Chu, and C.C. Sun, *Homology modelling and molecular dynamics study of human fatty acid amide hydrolase*, Mol. Simul. 35 (2009), pp. 1201–1208.
[37] A.A. San Juan and S.J. Cho, *3D-QSAR study of microsomal prostaglandin E2 synthase (mPGES-1) inhibitors*, J. Mol. Model. 13 (2007), pp. 601–610.
[38] M.D. AbdulHameed, A. Hamza, J. Liu, X. Huang, and C.G. Zhan, *Human microsomal prostaglandin E synthase-1 (mPGES-1) binding with inhibitors and the quantitative structure–activity correlation*, J. Chem. Inf. Model. 48 (2008), pp. 179–185.
[39] C. Jegerschold, S.C. Pawelzik, P. Purhonen, P. Bhakat, K.R. Gheorghe, N. Gyobu, K. Mitsuoka, R. Morgenstern, P.J. Jakobsson, and H. Hebert, *Structural basis for induced formation of the inflammatory mediator prostaglandin E2*, Proc. Natl. Acad. Sci. USA 105 (2008), pp. 11110–11115.
[40] G. Mbalaviele, A.M. Pauley, A.F. Shaffer, B.S. Zweifel, S. Mathialagan, S.J. Mnich, O.V. Nemirovskiy, J. Carter, J.K. Gierse, J.L. Wang, M.L. Vazquez, W.M. Moore, and J.L. Masferrer, *Distinction of microsomal prostaglandin E synthase-1 (mPGES-1) inhibition from cyclooxygenase-2 inhibition in cells using a novel, selective mPGES-1 inhibitor*, Biochem. Pharmacol. 79 (2010), pp. 1445–1454.
[41] M.D. Guerrero, M. Aquino, I. Bruno, R. Riccio, M.C. Terencio, and M. Paya, *Anti-inflammatory and analgesic activity of a novel inhibitor of microsomal prostaglandin E synthase-1 expression*, Eur. J. Pharmacol. 620 (2009), pp. 112–119.
[42] T. Hammarberg, M. Hamberg, A. Wetterholm, H. Hansson, B. Samuelsson, and J.Z. Haeggstrom, *Mutation of a critical arginine in microsomal prostaglandin E synthase-1 shifts the isomerase activity to a reductase activity that converts prostaglandin H2 into prostaglandin F2alpha*, J. Biol. Chem. 284 (2009), pp. 301–305.
[43] X. Huang, W. Yan, D. Gao, M. Tong, H.H. Tai, and C.G. Zhan, *Structural and functional characterization of human microsomal prostaglandin E synthase-1 by computational modeling and site-directed mutagenesis*, Bioorg. Med. Chem. 14 (2006), pp. 3553–3562.
[44] L. Xing, R.G. Kurumbail, R.B. Frazier, M.S. Davies, H. Fujiwara, R.A. Weinberg, J.K. Gierse, N. Caspers, J.S. Carter, J.J. McDonald, W.M. Moore, and M.L. Vazquez, *Homo-timeric structural model of human microsomal prostaglandin E synthase-1 and characterization of its substrate/inhibitor binding interactions*, J. Comput. Aided Mol. Des. 23 (2009), pp. 13–24.
[45] A. Hamza, M. Tong, M.D. AbdulHameed, J. Liu, A.C. Goren, H.H. Tai, and C.G. Zhan, *Understanding microscopic binding of human microsomal prostaglandin E synthase-1 (mPGES-1) trimer with substrate PGH2 and cofactor GSH: Insights from computational alanine scanning and site-directed mutagenesis*, J. Phys. Chem. B 114 (2010), pp. 5605–5616.
[46] Y.J. Tang, J.S. Yang, C.F. Lin, W.C. Shyu, M. Tsuzuki, C.C. Lu, Y.F. Chen, and K.C. Lai, *Houttuynia cordata Thunb extract induces apoptosis through mitochondrial-dependent pathway in HT-29 human colon adenocarcinoma cells*, Oncol. Rep. 22 (2009), pp. 1051–1056.
[47] C.R. Su, Y.F. Chen, M.J. Liou, H.Y. Tsai, W.S. Chang, and T.S. Wu, *Anti-inflammatory activities of furanoditerpenoids and other constituents from Fibraurea tinctoria*, Bioorgan. Med. Chem. 16 (2008), pp. 9603–9609.
[48] Y.H. Hsieh, F.H. Chu, Y.S. Wang, S.C. Chien, S.T. Chang, J.F. Shaw, C.Y. Chen, W.W. Hsiao, Y.H. Kuo, and S.Y. Wang, *Antrocamphin A, an anti-inflammatory principal from the fruiting body of taiwanofungus camphoratus, and its mechanisms*, J. Agr. Food Chem. 58 (2010), pp. 3153–3158.